Nanoscale

Accepted Manuscript

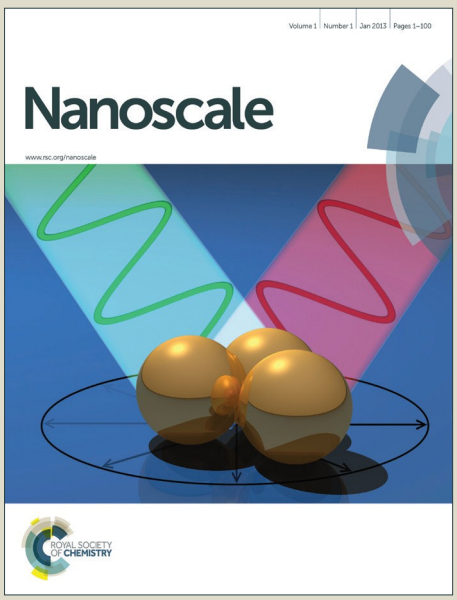

ROYAL SOCIETY OF CHEMISTRY

www.rsc.org/nanoscale

Journal Name

RSCPublishing

ARTICLE

Nitrogen and Phosphorus co-doped Graphene Quantum Dots: Synthesis from Adenosine triphosphate, Optical Properties, and Cellular Imaging

Cite this: DOI: 10.1039/x0xx00000x

Received 00th January 2012,
Accepted 00th January 2012

DOI: 10.1039/x0xx00000x

www.rsc.org/

Arundithi Ananthanarayanan[a], Yue Wang[b], Parimal Routh[a], Mahasin Alam Sk[a], Aung Than[a], Ming Lin[c], Jie Zhang[c], Jie Chen[a], Handong Sun[b] and Peng Chen[a]*

Graphene quantum dots (GQDs) are emerging zero-dimensional materials promising a wide spectrum of applications, particularly, as superior fluorescent reporters for bio-imaging and optical sensing. Heteroatom doping can endow GQDs with new or improved photoluminescence properties. Here, we demonstrate a simple strategy for the synthesis of nitrogen and phosphorous co-doped GQDs from a single biomolecule precursor (adenosine triphosphate - ATP). Such ATP-GQDs exhibit high fluorescence quantum yield, strong two-photon upconversion, small molecular weight, high photostability, and good biocompatibility. Furthermore, transferrin conjugated ATP-GQDs have been used for imaging and real-time tracking of transferrin receptors in live cells.

Introduction

Graphene quantum dots (GQDs) are a new class of zero-dimensional nanomaterials, which have shown immense potentials for bioimaging, optical sensing, energy conversion, and catalysis.[1-4] Owing to their tunable photoluminescence (PL), photostability, molecular size, biocompatibility, and ease to be conjugated with biomolecules, GQDs are particularly attractive for bioimaging.[5-15] It has been shown that heteroatom doping can endow GQDs with tailored or new PL as well as other properties.[15-17] Heteroatom-doped GQDs can be synthesized by exfoliating pre-doped graphene or graphene oxide sheets. [18-21] But such top-down methods are tedious because of the need of multiple steps and are usually of low doping efficiency. Alternatively, doped GQDs can be obtained by pyrolyzing small organic molecules, with heteroatoms naturally inherited from the precursor molecules. [22-25]

Herein, we report a simple and cost-effective method for the synthesis of GQDs co-doped with nitrogen, and phosphorus by carbonization and subsequent chemical exfoliation of a single precursor molecule - adenosine triphosphate (ATP) (Scheme 1, also see experimental section). The dually-doped GQDs show high quantum yield (~27.5%) and strong two-photon excitation with a two-photon absorption cross section (20000 GM). Carbonaceous micro-sheets resulted from ATP carbonization exhibits good catalytic properties towards oxygen reduction. And conjugated with transferrin, heteroatom-doped GQDs have been employed to image and track transferrin receptors in live cells.

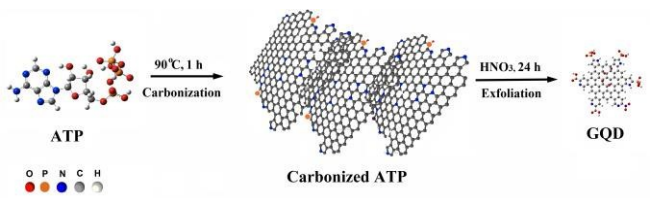

Scheme 1. Illustration of the synthesis procedure for ATP-GQDs.

Results and discussion

Adenosine triphosphate (ATP) is universal energy currency in cells, containing cyclic carbon rings, nitrogen, phosphorus, and oxygen atoms. Carbonization of ATP molecules yields porous aggregates of carbonaceous micro-sheets (Figure 1a), resulting from re-organization and fusion of the precursor molecules. Raman spectrum of the carbonized ATP (cATP) show prominent D and G bands (Figure 1b), suggesting its graphitic nature with the presence of sp^3 carbon due to covalent bonding with heteroatoms. Heteroatom doping is able to confer the inert graphene or graphitic materials with catalytic abilities.[16, 26] Indeed, cATP exhibits good catalytic properties towards oxygen reduction (ORR) as evidenced by the prominent reduction peak at ~ -0.26 V in the presence of oxygen (Figure 1c). Linear sweep voltammograms of cATP in oxygen-saturated 0.1M KOH are obtained using a rotating disk electrode at various rotating speeds to determine the number of electrons transferred for the ORR process (Figure 1d). Koutecky–Levich (K–L) plots at different potentials are plotted in Figure 1d inset. The slopes of the K-L curves suggest that the ORR process catalyzed by cATP is highly efficient through the 4-electron reduction pathway. Furthermore, the onset potential of cATP electrode is around -0.14 V, which is desirably lower than the previously reported N-doped graphene.[27-30] This experiment suggests that cATP is heteroatom-doped and its potential for fuel cell applications.

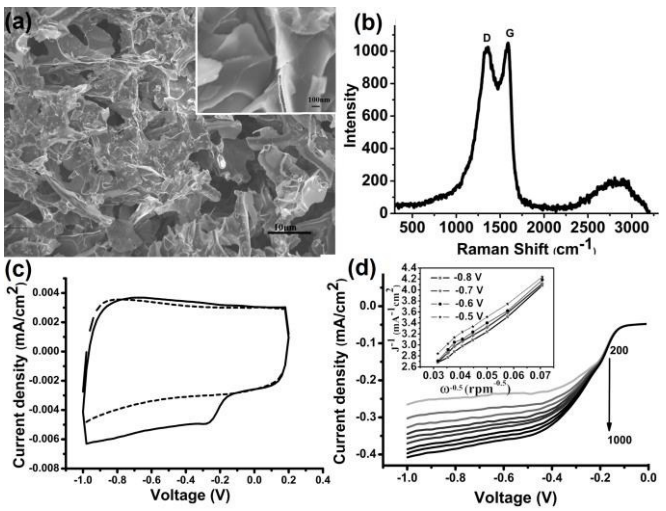

Figure 1. a) SEM images of carbonized ATP (cATP). The inset shows the surface of cATP sheets at higher magnification. b) Raman spectrum of carbonized ATP. c) Cyclic voltammograms of cATP in oxygen (solid line) or nitrogen (dotted line) saturated KOH (0.1 M) solution. d) Linear-sweep voltammetry curves of cATP in 0.1 M KOH at different rotation speeds. Inset is the Koutecky-Levich plots at different potentials (the slopes of the curves indicate the electron transfer number of 4.2 - 4.4).

Subsequently, cATP is exfoliated by refluxing in nitric acid. As revealed by transmission electron microscopy (TEM), carbon nanosheets ~2.06 (±0.69, n = 161) in diameter have been produced (Figure 2a & b). The high-resolution TEM image shows the lattice spacing of 0.24 nm corresponding to the d1120 plane of graphene (Figure 2a inset). Gel electrophoresis also indicates that the obtained nanosheets have a narrow size-distribution and small molecular weight (<< 10 kDa) (Figure 2c). Atomic force microscopy (AFM) reveals that the average thickness of these carbon particles is ~1.26 nm (± 0.66, n =231) corresponding to 1-3 layers of graphitic carbon (Figure 2b & c). These observations demonstrate that cATP exfoliation yields a nearly homogenous dispersion of GQDs.

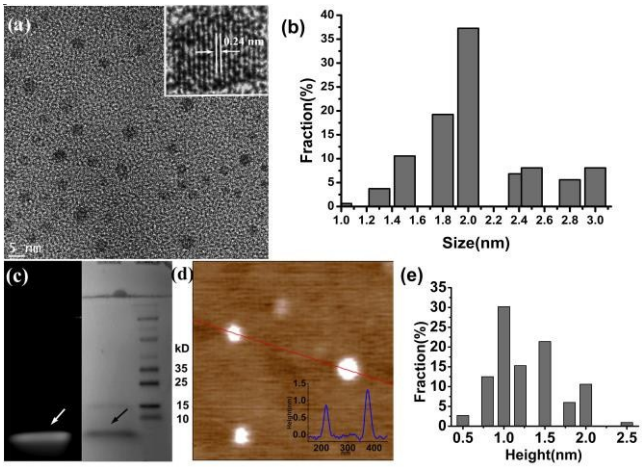

Figure 2. (a) TEM image of ATP-GQDs. The HR-TEM image in inset reveals the lattice spacing. (b) Size distribution histogram from TEM images (161 samples). (c) Gel electrophoresis images of ATP-GQD samples (left: excitation at 488 nm; right: bright view; arrows indicate the ATP-GQD band). On the right of the bright-field image, there are the electrophoretic bands of protein markers with indicated molecular weights. (d) AFM image of GQDs with the height profile along the indicated line shown in inset. (e) Height distribution obtained from 213 samples.

Fourier transform infrared spectroscopy (FTIR) spectrum of ATP-GQD shows the characteristic peaks for C=O (1722 cm^{-1}), C=C (1629cm^{-1}), OH (3414cm^{-1}), -COOH (1388cm^{-1}), P-O (966 cm^{-1}) and CH_2 (2922 cm^{-1}) (Figure 3a). On further characterization with X-ray photoelectron spectroscopy (XPS), the high resolution C^{1s} spectrum of GQDs can be well-fitted with the characteristic peaks for C=C bonds (284.2 eV),[31] C-N/ C-P=O (285.1eV), [19, 32] C-O (286.3 eV) [33] and O-C=O (288.2 eV)[19] (Figure 3b). It correlates well with the FTIR results. The N^{1s} spectrum consists of three peaks at 399.3, 400.5 and 405.1 eV, corresponding to the pyridinic,[34] pyrrolic,[34] and NO_2 groups, respectively (Figure 3c). The NO_2 groups are likely introduced at the edges during the exfoliation with HNO_3. Analysis of the P^{2p} XPS spectrum gives two peaks at 132.6 eV and 133.5 eV (Figure 3d), which can be assigned to P-O and P-C bond.[35, 36] It is likely that these bonds belong to phosphonic acid groups (-PO_3H_2) at the edges because incorporation of P in the graphene lattice would introduce unstable structural distortion due to the longer length of P-C bond than that of C-C or C-N bond.[37] As reported by XPS, the doping percentage of nitrogen and phosphorous are 6.2 (C/N ratio of 7.0) and 6.9 (C/P ratio of 6.3), respectively. Evidently, ATP-GQDs are doped with both N and P atoms. P-doped GQDs have yet to be synthesized so far. And this is the first demonstration of P-/N- co-doping. The N-doping level here is higher than the previously

reported N-/B- co-doped GQDs.[38] The interlayer spacing of ATP-GQDs analyzed by X-ray diffraction (XRD) is ~0.36 nm (Figure S1a), which is slightly larger than that of graphite (0.34 nm) due to the presence of chemical groups. The Raman spectrum of ATP-GQD is similar to that of cATP (Figure S1b).

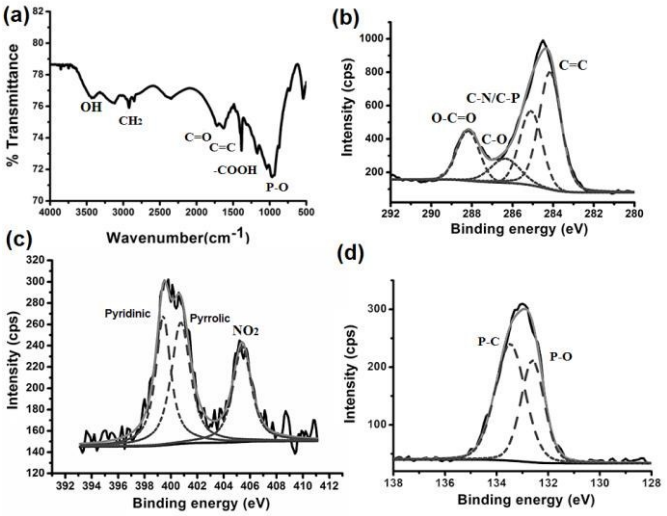

Figure 3. (a) FTIR spectrum of ATP-GQDs. (b, c, d) High resolution XPS spectra for C^{1s}, N^{1s}, and P^{2p}.

ATP-GQDs appear brown under bright light and show green fluorescence on illumination with 365 nm UV lamp (Figure 4a, inset). From the UV-Vis spectrum, it can be seen that, with adsorption extends to visible light regime, ATP-GQDs can more efficiently absorb short-wavelengths due to π–π* transitions of the aromatic sp^2 domains in the graphene lattice[31] (Fig. 4a). The photoluminescence (PL) excitation spectrum shows a prominent peak at 460 nm and a shoulder peak at 360 nm which is due to the σ – π and π–π* transitions originated from the carbene like triplet state of the zig-zag edges of GQDs (Figure 4a).[39]

In contrast to most reported GQDs,[40-42] the PL of ATP-GQDs only exhibits a slight excitation dependent emission with maximum emission at 520 nm when excited at 460 nm (Figure 4b and Figure S2). It suggests the good uniformity of size and chemical composition of our ATP-GQDs.[17] The quantum yield (QY) is calculated to be ~27.5% using rhodamine 6G (QY 96%) as the reference, which is much higher than the non-doped GQDs.[40] The improved QY could be attributable to the interplay of the different dopants in the graphene lattice. It has been proposed that coexistence of n- and p-dopants can increase QY due to formation of p-n type photochemical diodes.[43] In ATP-GQD, pyridinic and pyrrolic N atoms are strongly electron withdrawing conferring p-type doping characteristics.[44] The electron-withdrawing $-PO_3H_2$ groups impose p-doping effects.[45] Additionally, the presence of oxygenated groups at the edges also give rise to either weak n- (e.g., -OH) or p- (e.g., -COOH) doping effects.[43]

It is known that oxygenated groups on GQDs compromise QY because of non-radiative recombination at these sites.[46] Li et. al. have demonstrated that greenish-yellow luminescent GQDs prepared *via* a microwave-assisted method become blue with an much improved QY (from 11.7 to 22.9%).[47] Consistently, we show that chemical reduction of ATP-GQDs using $NaBH_4$ can largely increase QY to 53%, and at the same time, blue-shift the emission peak to ~475 nm (Figure S3a). But the emission spectrum is broadened, presumably due to increased chemical heterogeneity after reduction. From the FTIR spectrum (Figure S3b), it can be observed that the -COOH, C=O, and P-O groups are eliminated by reduction while -OH groups are still present because of reduction of -COOH to $-CH_2OH$. Clearly, the overall oxygen content is greatly decreased after chemical reduction. On the other hand, removing oxygenated groups makes GQDs more prone to aggregation and more difficult to be conjugated with biomolecules. Therefore, in the later bioimaging experiments, we use as-prepared ATP-GQDs without reduction.

Based on the chemical / element composition analyses and observed quantum dot size, we propose a hypothetical model for ATP-GQD (Figure S4) and theoretically investigate its PL properties using density-functional theory (DFT) and time-dependent DFT (TDDFT) calculations. The hypothetical ATP-GQD (~2 nm) contains 3 pyridinic N atoms, 3 pyrrolic N atoms, and 3 $-PO_3H_2$ groups. As the synthesized ATP-GQDs have rich oxygen content and to correlate with XPS characterization, 1 epoxy group is added onto graphene lattice, 1 $-NO_2$ and 2 -COOH are attached to pyridine rings. The TDDFT calculations suggest that ATP-GQD exhibits maximum emission at 556 nm which is close to the experimentally measured value (520 nm) (Figure S4a). Furthermore, our calculations suggest that chemical reduction (removal of oxygenated groups) can cause either red- or blue-shift (Figure S4 b-f), probably accounting for the observed broadening of the emission spectrum. In addition, it is likely that reduction pathway from Figure S4a-f dominates, giving an emission peak of 496.6 nm which is close to experimental value of 475 nm. The molecular weight of the hypothetical ATP-GQD is ~1.4kDa, which is much smaller than green fluorescence protein (GFP, ~27 kDa).

A major drawback of the currently used organic fluorophores (e.g., GFP and FITC) is their poor photostability, which makes long-term real-time imaging difficult. As shown in Figure S5, under the same confocal illumination, FITC photobleaches quickly whereas the PL of ATP-GQD remains stable. Because ATP molecules abundantly exist in cells, it is not surprising that ATP-GQDs show good biocompatibility at the concentrations much higher than needed for bioimaging experiments (Figure S6).

Furthermore, we examined the two-photon absorption properties of ATP-GQDs as two-photon fluorescence microscopy has advantageous over normal one-photon fluorescence microscopy in terms of larger penetration depth amenable for tissue imaging, higher spatial resolution and lower background signal due to highly non-linear and localized adsorption process.[48] Interestingly, ATP-GQD also exhibits good two-photon excitation properties. Under the excitation at 800 nm, which is far away from the one-photon absorption regime of GQD, strong upconverted PL is observed with emission maximum at ~560 nm (Figure 4c). The quadratic dependence of the PL signal on the excitation intensity confirms the nonlinear two-photon absorption and emission process (Figure 4d).[49] The Z-scan technique is employed to determine the two-photon absorption cross-section (σ) of our ATP-GQDs (Figure S7). The nonlinear absorption signal of the ATP-GQDs can be well-fitted by

the Z-scan theory,[49, 50] giving a σ as high as ~20000 GM. This value is two-orders higher than organic fluorphores[51] and comparable to much larger-sized CdSe quantum dots.[52]

Un-doped GQDs exhibit poor two-photon excitation properties due to low absorption cross-section.[53] It has been observed that two-photon absorption cross-section of quadrupolar molecules increases due to co-existence of electron withdrawing and donating groups which facilitates intramolecular charge transfer.[54] Theoretical study also suggests non-linear emission from GQDs could arise when electron-withdrawing NO_2 and electron-donating NH_2 groups at the edges forms a donor-GQD-acceptor system.[55] Liu et. al. have demonstrated that dimethyl amine functionalized GQD shows strong two-photon absorption and attributed this to the electron-donating nature of the dimethyl amine groups.[13] Hence conceivably, the co-existence of electron withdrawing and donating sites (which can form p-n type photochemical diodes) in heteroatom-doped ATP-GQD leads to its good two-photon upconversion properties.

ATP-GQD demonstrates excellent photostability under continuous one-photon or two-photon laser excitation (Figure S8). The lifetime measurements of ATP-GQDs under both one- (400 nm) and two-photon excitation show nearly identical PL decay dynamics (Figure S9), suggesting the common radiative recombination channels.[50] The PL decay curves can be well-fitted by a double-exponential function: $I_{(t)} = A_1 \exp(-t/\tau_1) + A_2 \exp(-t/\tau_2)$, where τ_1 and τ_2 are the time constants of the two radiative decay channels; A_1 and A_2 are the corresponding amplitudes. From the best-fit of the data, τ_1 (A_1) and τ_2 (A_2) are derived to be 320 ps (0.44) and 1.62 ns (0.56). The nanosecond-scale lifetime suggests that ATP-GQDs are suitable fluorescent probes for bio-imaging.[9]

ATP-GQD is desirable as a fluorescence tag for bioimaging because of its high QY, small molecular weight, excellent photostability, and good biocompatibility. A number of studies have provided proof-of-concept demonstrations to show the potential of GQDs for bioimaging, through simple non-specific cell imaging of passively up-taken GQDs. However, for useful biological studies, GQDs should be bio-functionalized for specific and real-time molecular imaging in live cells. Here, we conjugated ATP-GQD with transferrin molecule for imaging and real-time tracking of transferrin receptors in human cervical cancer cells (HeLa) cells. Many cancerous cells overexpress transferrin receptors, which are responsible for internalization and recycling of iron-bound transferrin molecules. Gel electrophoresis experiment indicates that the molecular weight of transferrin-conjugated GQD (Tr-GQD) is similar to that of bare transferrin molecule (80 kDa) implying one-to-one pairing between ATP-GQD and transferrin (Figure S10). The successful conjugation of transferrin is evidenced by staining of Tr-GQD by transferrin-binding coomassie blue (Figure S10).

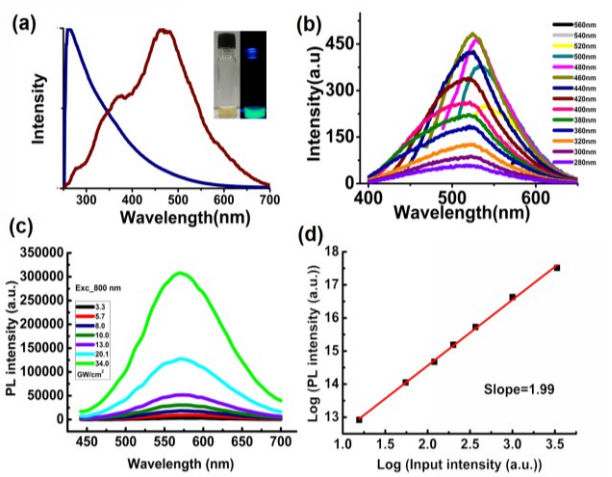

Figure 4. (a) UV-Vis absorption (blue) and excitation (red) spectra of GQDs. The inset shows the optical image of aqueous solution of ATP-GQDs under visible (left) and UV light (right, 365 nm). (b) PL spectra of GQDs at different excitation wavelengths. (c) Laser power dependent emission spectra of ATP-GQDs under two-photon excitation using a femtosecond pulsed laser (800 nm). (d) Quadratic relation between excitation intensity and PL intensity with a fitting (red line).

Using confocal microscopy, it is found that ATP-GQDs can be readily and non-specifically uptaken by HeLa cells (Figure 5a). The internalized ATP-GQDs scatter in the cytoplasm. In comparison, the uptaken Tr-GQDs are segregated near the nucleus because the specific binding of Tr-GQDs with transferrin receptors on the cell membrane triggers endocytosis and compartmentalization in the recycling endosomes (a network of tubular structures adjacent to the nucleus) as shown in Figure 5b.[56] When excess free transferrin molecules are introduced together with Tr-GQDs, fewer fluorescent puncta could be observed within the cells due to competitive inhibition, confirming the specific binding between Tr-GQDs and transferrin receptors (Figure 5c). Furthermore, Tr-GQD staining is much weaker in human fibroblasts (ATCC) because these non-cancerous cells have less transferrin receptors expressed. Using total internal reflection fluorescence microscopy (TIRFM) which evanescently illuminates only the thin plasmalemmal region (< 200 nm thick), it is further observed that Tr-GQD / transferrin complexes on the cell membrane are quickly endocytosed and many endocytic events are observed within 3 mins of imaging (Figure 5e). Individual endocytic (Figure 5e, right top) and exocytic events (Figure 5e, right bottom) of the vesicles containing internalized complexes can also be resolved.

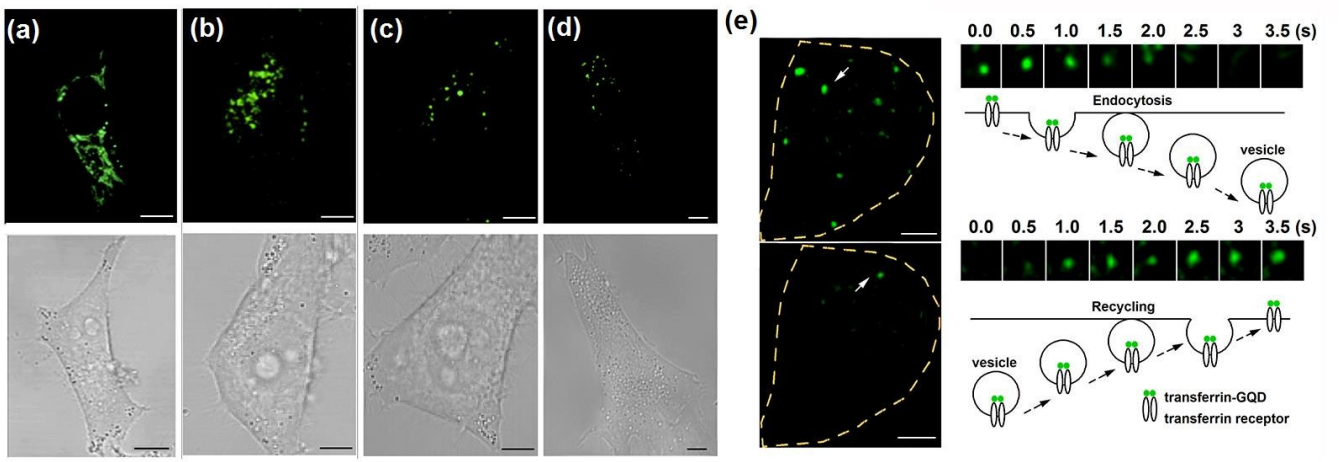

Figure 5. Confocal (top) and bright-field (bottom) images (Scale bars = 5 μm) of HeLa cells labeled with (a) ATP-GQDs, (b) Tr-GQDs, and (c) excess transferrin molecules together with Tr-GQDs. (d) Confocal and bright-field images of human fibroblast cells labeled with Tr-GQDs. (e) TIRFM images of HeLa cells with transferrin receptors labeled by Tr-GQDs (Scale bars = 5 μm). Right top: a typical endocytic event of Tr-GQD/transferrin receptor complexes; Right bottom: a typical exocytic event of a vesicle containing Tr-GQD / receptor complexes.

Experimental

Synthesis of ATP-GQDs

ATP powder (1g, Acros Organics) was carbonized by heating in a quartz tube furnace at 900°C for 1h in argon atmosphere. This was followed by refluxing in HNO_3 (6 M, Honeywell Chemicals) for 24 h. The solution was then cooled and centrifuged at 7500Xg for 20 min. The supernatant was collected and the excess HNO_3 was removed by evaporation at 200°C. The resulting powder was subsequently dissolved in DI water and dialyzed using a cellulose ester dialysis membrane (500-1000 Da MWCO, Spectra/Pro Biotec) for 2 days to remove ions and other impurities.

Oxygen reduction reaction (ORR)

The carbonized ATP samples were washed with DI water 6 times to remove ions or other impurities and dried at 50°C in a hot air oven. Carbonized ATP dispersion (2 mg/ml) was drop-casted onto a polished glassy carbon electrode. The ORR measurements were conducted with a CHI 660D electrochemical workstation (Chenhua), using nitrogen or oxygen saturated KOH (0.1 M) solution as the electrolyte.

Characterizations

Samples were characterized by field-emission scanning electron microscopy (JSM6700-FESEM, JEOL), Raman spectroscopy (WITeck CRM200), Atomic force microscopy (MFP-3D AFM, Asylum research), high-resolution transmission-electron microscopy (JEOL-2010), Fourier transform infrared spectroscopy (PerkinElmer Spectrum GX FTIR system), X-ray photoelectron spectroscopy (Theta Probe), X-ray diffraction analysis (Bruker D8 Advanced Diffraction meter using Cu Kα radiation), UV-vis absorption spectroscopy (UV-2450 spectrophotometer, Shimadzu), photoluminescence spectroscopy (LS-55 fluorescence spectrometer, PerkinElmer) and polyacrylamide gel electrophoresis and imaging (Mini-Protean Tetra Cell, Bio-Rad and ProXPRESS 2D, Perkin Elmer). The two-photon excited PL properties at 800 nm excitation were investigated using a femtosecond amplified-pulsed laser with repetition rate of 1000 Hz and pulse-width of 100 fs.[50] The lifetime measurements were carried out for the one and two-photon excitation by an Optronics streak camera system.[57]

Graphics should be inserted where they are first mentioned (unless they are equations, which appear in the flow of the text). They can be single column or double column as appropriate.

Cell Imaging

Human cervical cancer cells (HeLa, ATCC) were cultured in Dulbeccos modified eagle medium supplemented with 10% Fetal bovine serum (Gibco). For the imaging experiments, HeLa cells were seeded on a Lab-Tek II chambered cover glass and grown overnight. Prior to imaging, the cells were incubated with ATP-GQDs for 2 h or Tr-GQDs for 30 min at 37°C. The cells were rinsed thrice and incubated in the bath solution (150 mM NaCl, 5 mM KCl, 1.1 mM $MgCl_2$, 2.6 mM $CaCl_2$, 10 mM HEPES, and 10 mM glucose, pH 7.4) during imaging. Confocal microscope (Zeiss LSM 510) with a 63X oil objective and a 488 nm laser was used to obtain the confocal images. Time-lapse digital images were recorded using a Zeiss Axiovert-200M inverted total-internal-reflection fluorescence microscope system (Carl Zeiss, Germany) equipped with a 100x objective lens (numerical aperture, NA=1.45) and a charge coupled device (CCD) camera with pixel size of 0.248 □m. Using MetaMorph 6.3 (Universal Imaging Corp., Downingtown,

PA), time-lapse images of 361 frames (0.5 s/frame) were acquired at 37°C, and analyzed using ImageJ (National Institute of Health, US).

Conclusions

In summary, we have devised a simple strategy to synthesize N and P co-doped GQDs using a biomolecule (ATP) as the precursor. Such novel QD exhibits high brightness (QY ~27.5% and ~53.0% after chemical reduction), low molecular weight (~1.4 kDa), strong two-photon excitation property (absorption cross section as high as 20000 GM), excellent one-photon and two-photon stability, good biocompatibility, high water solubility, and ease to be conjugated with biomolecules. We further demonstrate the potential of ATP-GQD for real-time molecular tracking in live cells whereby uncovering the dynamic cellular events, in this case, distribution, trafficking, and recycling of transferrin receptors

Acknowledgements

We thank the support from Ministry of Education of Singapore under an AcRF Tier 2 grant (MOE2014-T2-2-003, ARC31/14) and Singapore National Research Foundation under its CBRG grant (NMRC/CBRG/0070/2014) administrated by the Singapore Ministry of Health's National Medical Research Council.

Notes and references

[a] Bioengineering Program, School of Chemical and Biomedical Engineering, Nanyang Technological University, 70 Nanyang Drive, Singapore 637457
E-mail: ChenPeng@ntu.edu.sg
[b] Division of Physics and Applied Physics, School of Physical and Mathematical Sciences, Nanyang Technological University, 21 Nanyang Link, Singapore 637371
[c] Institute of Materials Research and Engineering, A*STAR (Agency for Science, Technology and Research), 3 Research Link, Singapore 117602

Electronic Supplementary Information (ESI) available: Supplementary figures related to characterization, computational studies and protein conjugation are available. See DOI: 10.1039/b000000x/

1. L. Li, G. Wu, G. Yang, J. Peng, J. Zhao and J. J. Zhu, *Nanoscale*, 2013, **5**, 4015.
2. J. Shen, Y. Zhu, X. Yang and C. Li, *Chemical communications*, 2012, **48**, 3686.
3. H. Sun, L. Wu, W. Wei and X. Qu, *Materials Today*, 2013, **16**, 433.
4. Z. P. Zhang, J. Zhang, N. Chen and L. T. Qu, *Energ Environ Sci*, 2012, **5**, 8869.
5. M. M. Xie, Y. J. Su, X. N. Lu, Y. Z. Zhang, Z. Yang and Y. F. Zhang, *Mater Lett*, 2013, **93**, 161.
6. L. Lin and S. Zhang, *Chemical communications*, 2012, **48**, 10177.
7. D. B. Shinde and V. K. Pillai, *Chem-Eur J*, 2012, **18**, 12522.
8. X. Wu, F. Tian, W. X. Wang, J. Chen, M. Wu and J. X. Zhao, *J Mater Chem C*, 2013, **1**, 4676.
9. J. Peng, W. Gao, B. K. Gupta, Z. Liu, R. Romero-Aburto, L. Ge, L. Song, L. B. Alemany, X. Zhan, G. Gao, S. A. Vithayathil, B. A. Kaipparettu, A. A. Marti, T. Hayashi, J. J. Zhu and P. M. Ajayan, *Nano letters*, 2012, **12**, 844.
10. Y. Q. Dong, C. Q. Chen, X. T. Zheng, L. L. Gao, Z. M. Cui, H. B. Yang, C. X. Guo, Y. W. Chi and C. M. Li, *J Mater Chem*, 2012, **22**, 8764.
11. W. J. Xie, Y. Y. Fu, H. Ma, M. Zhang and L. Z. Fan, *Acta Chim Sinica*, 2012, **70**, 2169.
12. L. Zhang, Y. Xing, N. He, Y. Zhang, Z. Lu, J. Zhang and Z. Zhang, *Journal of nanoscience and nanotechnology*, 2012, **12**, 2924.
13. Q. Liu, B. Guo, Z. Rao, B. Zhang and J. R. Gong, *Nano letters*, 2013, **13**, 2436.
14. X. T. Zheng, A. Than, A. Ananthanaraya, D.-H. Kim and P. Chen, *ACS nano*, 2013, **7**, 6278.
15. X. T. Zheng, A. Ananthanarayanan, K. Q. Luo and P. Chen, *Small*, 2014. DOI 10.1002/smll.201402648
16. X. Wang, G. Sun, P. Routh, D.-H. Kim, W. Huang and P. Chen, *Chemical Society Reviews*, 2014, **43**, 7067.
17. M. A. Sk, A. Ananthanarayanan, L. Huang, K. H. Lim and P. Chen, *J Mater Chem C*, 2014, **2**, 6954.
18. Y. Li, Y. Zhao, H. H. Cheng, Y. Hu, G. Q. Shi, L. M. Dai and L. T. Qu, *Journal of the American Chemical Society*, 2012, **134**, 15.
19. M. Li, W. B. Wu, W. C. Ren, H. M. Cheng, N. J. Tang, W. Zhong and Y. W. Du, *Appl Phys Lett*, 2012, **101**.
20. T. Palaniselvam, M. O. Valappil, R. Illathvalappil and S. Kurungot, *Energ Environ Sci*, 2014, **7**, 1059;.
21. C. F. Hu, Y. L. Liu, Y. H. Yang, J. H. Cui, Z. R. Huang, Y. L. Wang, L. F. Yang, H. B. Wang, Y. Xiao and J. H. Rong, *J Mater Chem B*, 2013, **1**, 39.
22. J. Ju and W. Chen, *Biosensors and Bioelectronics*, 2014, **58**, 219.
23. D. Qu, M. Zheng, P. Du, Y. Zhou, L. Zhang, D. Li, H. Tan, Z. Zhao, Z. Xie and Z. Sun, *Nanoscale*, 2013, **5**, 12272.
24. D. Qu, M. Zheng, L. Zhang, H. Zhao, Z. Xie, X. Jing, R. E. Haddad, H. Fan and Z. Sun, *Sci. Rep.*, 2014, **4**.
25. L. Lin, M. Rong, S. Lu, X. Song, Y. Zhong, J. Yan, Y. Wang and X. Chen, *Nanoscale*, 2015, **7**, 1872.
26. H. Wang, T. Maiyalagan and X. Wang, *ACS Catalysis*, 2012, **2**, 781.
27. I.-Y. Jeon, H.-J. Choi, S.-M. Jung, J.-M. Seo, M.-J. Kim, L. Dai and J.-B. Baek, *Journal of the American Chemical Society*, 2012, **135**, 1386.
28. L. T. Qu, Y. Liu, J. B. Baek and L. M. Dai, *ACS nano*, 2010, **4**, 1321.
29. Z. J. Lu, S. J. Bao, Y. T. Gou, C. J. Cai, C. C. Ji, M. W. Xu, J. Song and R. Y. Wang, *Rsc Adv*, 2013, **3**, 3990.
30. Z. H. Sheng, L. Shao, J. J. Chen, W. J. Bao, F. B. Wang and X. H. Xia, *ACS nano*, 2011, **5**, 4350.
31. Y. Li, Y. Zhao, H. Cheng, Y. Hu, G. Shi, L. Dai and L. Qu, *Journal of the American Chemical Society*, 2012, **134**, 15.
32. S. H. Liao, P. L. Liu, M. C. Hsiao, C. C. Teng, C. A. Wang, M. D. Ger and C. L. Chiang, *Ind. Eng. Chem. Res.*, 2012, **51**, 4573.
33. H. Jabeen, V. Chandra, S. Jung, J. W. Lee, K. S. Kim and S. Bin Kim, *Nanoscale*, 2011, **3**, 3583.
34. Z. Luo, S. Lim, Z. Tian, J. Shang, L. Lai, B. MacDonald, C. Fu, Z. Shen, T. Yu and J. Lin, *J Mater Chem*, 2011, **21**, 8038-8044.
35. J. N. Hart, P. W. May, N. L. Allan, K. R. Hallam, F. Claeyssens, G. M. Fuge, M. Ruda and P. J. Heard, *Journal of Solid State Chemistry*, 2013, **198**, 466.
36. K. S. Prasad, R. Pallela, D. M. Kim and Y. B. Shim, *Part Part Syst Char*, 2013, **30**, 557.
37. H.-m. Wang, H.-x. Wang, Y. Chen, Y.-j. Liu, J.-x. Zhao, Q.-h. Cai and X.-z. Wang, *Applied Surface Science*, 2013, **273**, 302.
38. S. Dey, A. Govindaraj, K. Biswas and C. N. R. Rao, *Chemical Physics Letters*, 2014, **595**, 203.
39. Y. Li, Y. Hu, Y. Zhao, G. Shi, L. Deng, Y. Hou and L. Qu, *Advanced materials*, 2011, **23**, 776.
40. Y. Dong, C. Chen, X. Zheng, L. Gao, Z. Cui, H. Yang, C. Guo, Y. Chi and C. M. Li, *J Mater Chem*, 2012, **22**, 8764.
41. X. Wu, F. Tian, W. Wang, J. Chen, M. Wu and J. X. Zhao, *Journal of materials chemistry. C, Materials for optical and electronic devices*, 2013, **1**, 4676.
42. A. Ananthanarayanan, X. Wang, P. Routh, B. Sana, S. Lim, D.-H. Kim, K.-H. Lim, J. Li and P. Chen, *Advanced Functional Materials*, 2014, **24**, 3021.
43. T.-F. Yeh, C.-Y. Teng, S.-J. Chen and H. Teng, *Advanced materials*, 2014, **26**, 3297.
44. T. Schiros, D. Nordlund, L. Palova, D. Prezzi, L. Y. Zhao, K. S. Kim, U. Wurstbauer, C. Gutierrez, D. Delongchamp, C. Jaye, D.

Fischer, H. Ogasawara, L. G. M. Pettersson, D. R. Reichman, P. Kim, M. S. Hybertsen and A. N. Pasupathy, *Nano letters*, 2012, **12**, 4025.
45. I. Gillaizeau-Gauthier, F. Odobel, M. Alebbi, R. Argazzi, E. Costa, C. A. Bignozzi, P. Qu and G. J. Meyer, *Inorganic Chemistry*, 2001, **40**, 6073.
46. S. Zhu, J. Zhang, S. Tang, C. Qiao, L. Wang, H. Wang, X. Liu, B. Li, Y. Li, W. Yu, X. Wang, H. Sun and B. Yang, *Advanced Functional Materials*, 2012, **22**, 4732.
47. L.-L. Li, J. Ji, R. Fei, C.-Z. Wang, Q. Lu, J.-R. Zhang, L.-P. Jiang and J.-J. Zhu, *Advanced Functional Materials*, 2012, **22**, 2971.
48. G. S. He, L.-S. Tan, Q. Zheng and P. N. Prasad, *Chemical Reviews*, 2008, **108**, 1245.
49. Y. Wang, X. Yang, T. C. He, Y. Gao, H. V. Demir, X. W. Sun and H. D. Sun, *Appl Phys Lett*, 2013, **102**, 021917.
50. Y. Wang, V. D. Ta, Y. Gao, T. C. He, R. Chen, E. Mutlugun, H. V. Demir and H. D. Sun, *Advanced materials*, 2014, **26**, 2954.
51. W. R. Zipfel, R. M. Williams and W. W. Webb, *Nature Biotechnology*, 2003, **21**, 1369.
52. S.-C. Pu, M.-J. Yang, C.-C. Hsu, C.-W. Lai, C.-C. Hsieh, S. H. Lin, Y.-M. Cheng and P.-T. Chou, *Small*, 2006, **2**, 1308.
53. A. Zhu, C. Ding and Y. Tian, *Scientific Reports*, 2013, **3**, 2933.
54. W.-H. Lee, M. Cho, S.-J. Jeon and B. R. Cho, *The Journal of Physical Chemistry A*, 2000, **104**, 11033.
55. Z.-J. Zhou, Z.-B. Liu, Z.-R. Li, X.-R. Huang and C.-C. Sun, *The Journal of Physical Chemistry C*, 2011, **115**, 16282.
56. A. Nagabhushana, M. L. Chalasani, N. Jain, V. Radha, N. Rangaraj, D. Balasubramanian and G. Swarup, *BMC cell biology*, 2010, **11**, 4.
57. Y. Wang, K. S. Leck, V. D. Ta, R. Chen, V. Nalla, Y. Gao, T. He, H. V. Demir and H. Sun, *Advanced materials*, 2015, **27**, 169.